Available online at www.sciencedirect.com
ScienceDirect
Trans. Nonferrous Met. Soc. China 33(2023) 3673−3684
Transactions of Nonferrous Metals Society of China
www.tnmsc.cn

Enhancing tensile properties of extruded AZ31 rod by introducing gradient bimodal microstructure

Qi SHANG[1], Fan WU[1], Hong-bing CHEN[2], Hong-ju ZHANG[3],
Ting-ting LIU[1], Ning GUO[1], Sheng-feng GUO[1], Bo SONG[1]

1. School of Materials and Energy, Southwest University, Chongqing 400715, China;
2. College of Engineering and Technology, Southwest University, Chongqing 400715, China;
3. Analytical & Testing Center, Southwest University, Chongqing 400715, China

Received 29 May 2022; accepted 31 August 2022

Abstract: The Mg alloy rods with a gradient bimodal microstructure were fabricated by forward-reverse torsion at 350 °C. The effects of the bimodal microstructure on tensile properties and deformation mechanism of the alloy were investigated in detail. The formation of gradient bimodal microstructure was attributed to the incomplete dynamic recrystallization and the characteristic of torsion deformation. The bimodal structure had less influence on the yield strength but largely increased the peak stress and tension ductility. The large heterogeneous deformation-induced strengthening via gradient bimodal microstructure was responsible for the enhanced strain hardening capacity and tensile ductility. Finally, the related deformation mechanisms were discussed.

Key words: Mg alloys; hot torsion; bimodal microstructure; heterogeneous deformation; tensile properties

1 Introduction

With the increasingly serious problems of world energy crisis, resource crisis and environmental pollution, energy saving and light weight have become important issues that need to be solved urgently in the automotive, aerospace and other industrial fields. Mg alloys, as the lightest metal structural material, their development and application have become an effective strategy to overcome the above problems. However, low strength and limited ductility become important bottlenecks restricting the application of Mg alloys [1]. Plastic processing can effectively refine the grains to improve the strength and toughness [2−5]. However, the formation of strong deformation texture leads to large plastic anisotropy in wrought Mg alloys. Further grain refinement and texture control have become the focus of research in the development of high-performance wrought Mg alloys [6−11].

Besides, more and more researches have focused on the development of Mg alloys with heterostructures [12−14]. This is because heterostructures can evade the strength−ductility trade-off dilemma. Heterostructures contain some domains with dramatic difference in strength, resulting in the deformation incompatibility during the deformation and significant hetero-deformation induced (HDI) hardening. HDI hardening can increase strength and strain hardening [15,16]. Thus, heterostructures offer a new strategy to simultaneously improve strength and ductility. Based on this, some typical heterostructures have been developed in various metals and alloys, such as heterogeneous lamella structure, gradient structure, bimodal structure, and dual-phase structure [15−18]. Recently, the construction of heterostructures has also received extensive attention in Mg alloys. LIU et al [12] obtained an AZ91 sheet with a heterogeneous

Corresponding author: Ting-ting LIU, E-mail: ttliu@swu.edu.cn; Bo SONG, Tel: +86-23-68253204, E-mail: bosong@swu.edu.cn
DOI: 10.1016/S1003-6326(23)66362-9

lamella structure by the combination of aging and low-temperature extrusion. WANG et al [19] fabricated the Mg alloy sheet with a lamella heterostructure by co-extrusion of Mg−Al−Zn alloy and Mg−Y alloy. ZHANG et al [20] reported a bimodal structured Mg−8Al−2Sn−1Zn alloy fabricated by hard-plate-rolling. WANG et al [21] studied the deformation mechanism of a bimodal structured AZ31 alloy. These results demonstrate that the formation of heterostructures is very beneficial to simultaneously improving the strength and tensile ductility of Mg alloys.

Recently, torsion deformation has been used to prepare the rods with gradient structures. As a simple plastic processing technique, it can be an important supplementary processing technology. This method has been used to process the Mg alloys [22,23], copper alloys [24,25], high entropy alloys [26,27], and steel [28,29]. It is found that the gradient deformation structure (such as gradient dislocations [24,27], gradient stacking fault [25], and gradient nano-twins [28]) introduced by room temperature torsion is of great significance in improving the strength and toughness of metal rods. In above reports, torsion deformation was usually performed at room temperature. However, the effect of hot torsion on mechanical properties was rarely reported. Firstly, hot torsion can induce dynamic recrystallization (DRX) [30,31]. The incomplete recrystallization is usually used to construct bimodal structures [20,21]. Secondly, the gradient shear stress of torsional deformation is beneficial to the construction of gradient microstructure. It is considered that the gradient recrystallization behavior via hot torsion can be exploited to build a gradient bimodal structure.

Based on this, hot torsion deformation was used to construct the gradient bimodal structure in the extruded AZ31 rod in this work. The effects of hot torsion deformation on the microstructure and recrystallization behavior of AZ31 alloy were investigated, and the effect of gradient bimodal structure on tensile properties was also analyzed. The related mechanisms were discussed.

2 Experimental

In this work, the extruded AZ31 alloy (Mg−2.87wt.%Al−0.95wt.%Zn) rods with a diameter of 10 mm were used as the starting materials. In order to remove dislocations and homogenize the structure, the extruded samples were annealed at 500 °C for 0.5 h. The as-extruded and annealed rods are named as AE sample. Dog-bone-shaped samples with a gauge size of *d*4 mm × 25 mm were prepared for the free-end torsion. The AE sample was held at 350 °C for 5 min and then subjected to hot torsion processing at 0.13 r/min. The torsional axis is parallel to the extrusion direction (ED). For the AE sample, the maximum torsion angle before fracture can achieve to 2000°. In this study, the 900° forward torsion (FT) and 900° forward-reverse torsion (FRT) were carried out to process the AE sample, and these twisted samples were denoted as FT and FRT samples, respectively.

After torsion, the twisted sample was directly used for the tensile test. Tensile tests at room temperature along the ED were carried out at a constant strain rate of $1\times10^{-3}\ s^{-1}$. Metallographic experiments were used to analyze the grain size. Microstructures were characterized using the electron backscatter diffraction (EBSD) of a JEOL 7800F FEG−SEM. EBSD measurements were executed on longitudinal sections of the samples (parallel to the axis of the rod) and the characterized regions were the edge and middle of rods. Loading−unloading−reloading tests during tensile tests were carried out at a strain rate of $1\times10^{-3}\ s^{-1}$ and room temperature. At a specific unloading strain, the specimen was unloaded in a load-control mode at an unloading rate of 1000 N/min, followed by reloading to the same applied load.

3 Results and discussion

AE sample exhibits a typical extrusion texture and has a uniform microstructure and coarse grains, as shown in Fig. 1(a). Considering that the torsional deformation will lead to the maximum shear strain at the edge of the twisted rod, the edge position of the torsion sample is selected to investigate the changes in the microstructure. Figure 1(b) shows the EBSD map and basal pole figure of FT sample. It is found that a remarkable texture change is caused by hot torsion. In the pole figures, the normal of the projection is the *r*-axis, the shear direction is the θ-axis and the axial direction is the *Z*-axis (i.e., ED direction). After hot torsion of 900°, the *c*-axis of the main texture component is located

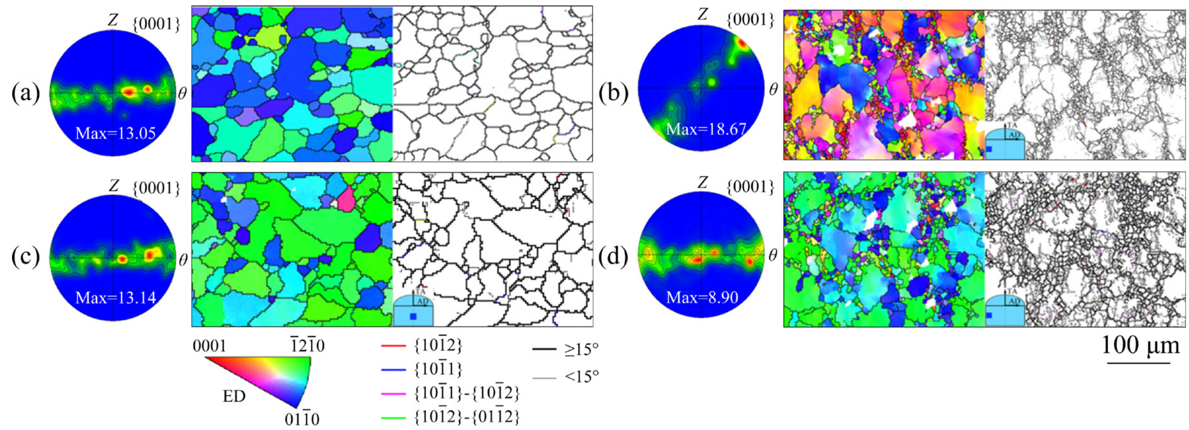

Fig. 1 EBSD data of AE sample (a), edge position of FT sample (b), center (c), and edge (d) positions of FRT sample

at 45° from *Z*-axis and *θ*-axis, as shown in Fig. 1(b). In the EBSD maps of twisted samples, no twins can be detected due to the high torsion temperature. Such a large textural change is mainly attributed to activation of basal slip during hot torsion [32]. According to previous studies, torsion deformation will cause *c*-axis of texture to rotate towards the *Z*-axis [30,33]. The forward-reverse torsion can restore the initial extruded texture due to the inverse shear directions between forward torsion and reverse torsion [34]. In this work, the forward-reverse torsion of 900° was performed to restore the initial texture, as shown in Figs. 1(c) and (d).

A large number of fine DRXed grains can also be generated during hot torsion. Clusters of low-angle grain boundaries within grains will cause the generation of sub-grains, which is the formation of continuous dynamic recrystallization. Discontinuous dynamic recrystallization was characterized by the bulge of the original high angle grain boundary [35,36]. In the FRT sample, a large misorientation and strong lattice distortion can be found within initial grains. Moreover, profuse bulges of grain boundaries can be found. Thus, for the AE sample, both continuous dynamic recrystallization and discontinuous dynamic recrystallization are the main DRX mechanisms during torsion at 350 °C. The fine DRXed grains are mainly formed at the grain boundaries, and a bimodal microstructure in which coarse grains are surrounded by fine recrystallized grains is fabricated by hot torsion. For the edge positions of FT and FRT samples, the accumulated equivalent strain can achieve 0.73 and 1.46, respectively. However, the degree of recrystallization is far lower than that of hot compression or hot tension [37,38]. It has been reported that the DRX process is related to the activation of deformation mechanism [39]. In this work, the dominated deformation mechanism is the basal slip during forward-reverse torsion [32]. The preferential activation of basal slip will delay the progress of recrystallization during the hot deformation [39]. This may be the main reason for the small amount of recrystallized grains in the FRT sample. Torsion deformation will also generate a gradient microstructure due to its deformation characteristics [30], as shown in Figs. 1(c) and (d). In order to visually display the distribution of the bimodal structure, optical microscope (OM) images of FRT sample across the radius direction are shown in Fig. 2. It indicates that a bimodal structure exhibits a gradient distribution. From edge position to center position, the area fraction of fine DRXed grains gradually decreases.

Figure 3(a) shows the true stress−strain curves of different samples. The yield strength (YS), peak strength (PS) and uniform elongation (UE) are listed in Table 1. For AE sample, the yield strength is 198 MPa and the uniform elongation is 12.6%. After hot torsion, the YS exhibits little change, while the PS is increased from 283 to 299 MPa and the uniform elongation is increased from 12.6% to 15.6%. Moreover, the static toughness (ST) is also calculated to estimate the amount of energy per unit volume of which the material can absorb without rupturing. The FRT increases the ST from 38 to 45 MJ/m^3. Thus, FRT torsion exhibits little influence on yield strength, but largely increases the peak strength, tensile ductility and static toughness. Figure 3(b) shows the strain hardening rate curves.

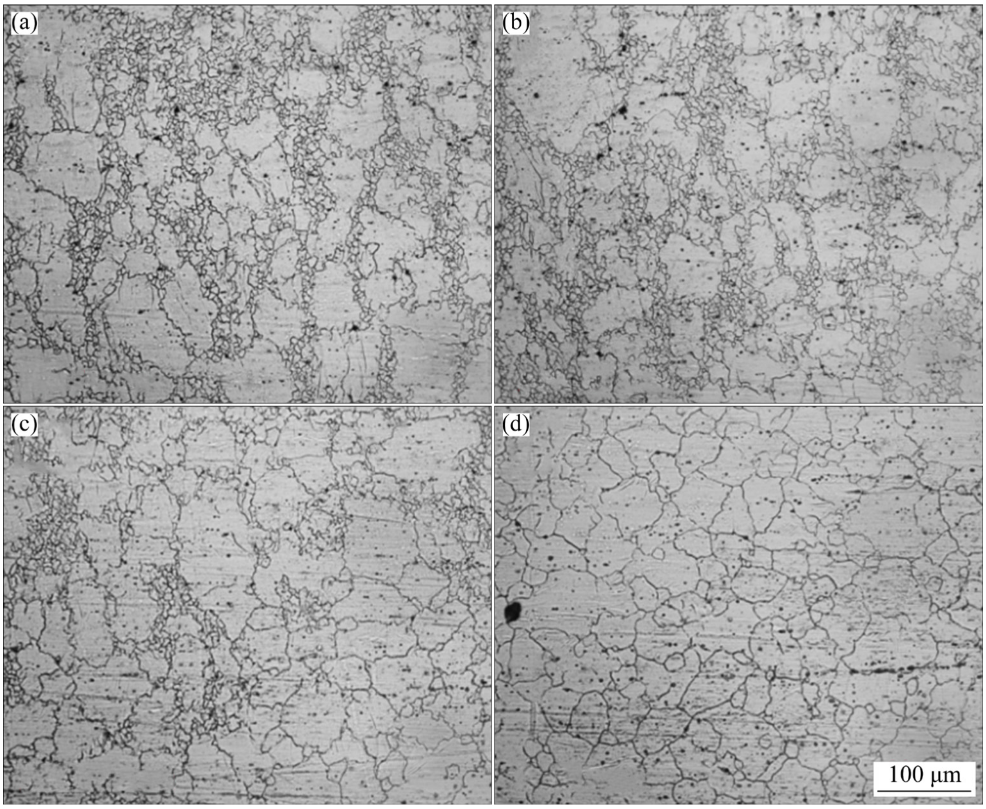

Fig. 2 OM images of FRT sample at various radial positions: (a) 2 mm (Edge position); (b) 1.5 mm; (c) 1.0 mm; (d) 0 mm (Center position)

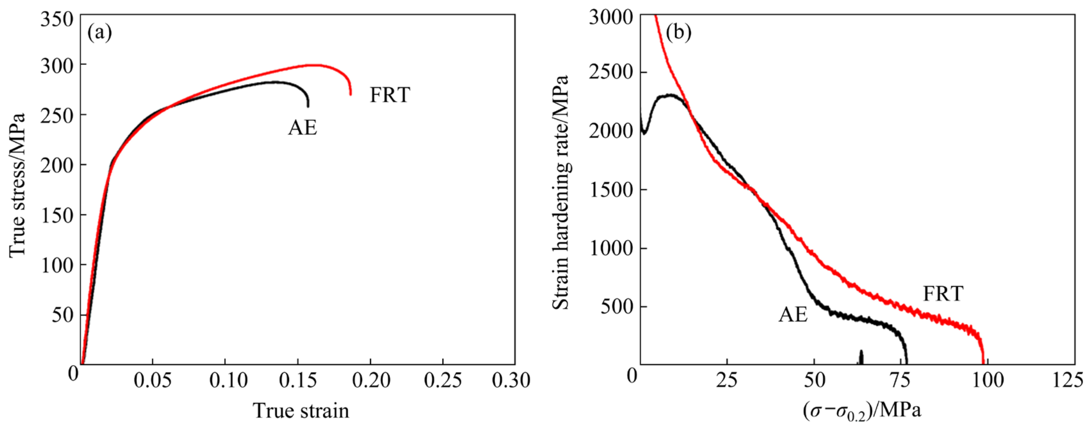

Fig. 3 True stress−strain curves (a) and corresponding strain hardening rate curves (b) of AE and FRT samples (σ is true stress, and $\sigma_{0.2}$ is yield stress)

Table 1 Tensile properties of various samples

Sample	YS/MPa	PS/MPa	UE/%	ST/(MJ·m^{-3})
AE	198±3	283±1	12.6±0.1	38±0.2
FRT	193±1	299±2	15.6±1.5	45±4.3

After elastic-plastic transition, a linear decrease in strain hardening behavior can be found in two samples. It is found that hot torsion largely reduces the slope of strain hardening rate curve.

The dislocation substructure, precipitates, texture and grain size are the main factors to determine the yield strength for Mg alloys. For AZ31 alloys, the $Mg_{17}Al_{12}$ phases are very rare due to the low Al content. Therefore, the contribution of precipitation strengthening is rarely considered in AZ31 alloys [8,9]. Moreover, Al−Mn phases are usually observed in AZ31 alloys [6]. However, few studies have reported that these phases have a significant effect on the room temperature strength of AZ31. Therefore, in this study, the influence of second phases on mechanical properties will not be considered.

During hot torsion at 350 °C, the dislocation substructure will be formed to generate profuse low-angle grain boundaries (LAGBs). In the EBSD map, the LAGBs (<15°) densities can be calculated by a previous method [40]. After torsion, LAGBs density is increased from 0.004 to 0.018 μm^{-1} and 0.068 μm^{-1} for the center position and edge position, respectively. In fact, the LAGBs density is still low owing to the strong dynamic/static recovery during hot torsion at 350 °C. The LAGBs density is comparable with that of the annealed samples [40]. Moreover, the LAGBs act as a weaker barrier to dislocation motion than the high-angle grain boundaries (HAGBs). It is considered that the dislocation hardening effect might be very limited.

The DRX-induced grain refinement can generate refinement hardening effect. Figure 4 shows the area fraction of grains as a function of grain size. For the AE sample, 96% of the grains are above 15 μm and the average grain size is ~25.5 μm, as shown in Fig. 4(a). Hot torsion largely increases the area fraction of grains with size below 15 μm. A typical bimodal grain distribution can be found at the edge position of FRT sample, as shown in Fig. 4(b). Here, the grains with sizes below 15 μm are recognized as DRXed grains. According to EBSD result, the DRXed grains have an average size of 6.8 μm at the edge position of FRT sample. According to Hall−Petch law, a reduction in grain size serves to enhance yield strength as formulated by [41]

$$\sigma_{HP}=\sigma_0+kd^{-0.5} \tag{1}$$

where σ_{HP} is the yield strength via Hall−Petch, σ_0 is the lattice friction stress, d is the average grain size, and k is the stress concentration factor. The increment of yield strength can be calculated by the formula: $\Delta\sigma=k(d_2^{-0.5}-d_1^{-0.5})$, where $\Delta\sigma$ is the increment of yield strength, d_1 is the initial grain size, and d_2 is the refined grain size. The k value is relevant to texture and deformation mechanism in Mg alloys [41,42]. For the extrusion rods with fiber texture, k is selected from a recent report [42]. The k value is 235 MPa·$\mu m^{1/2}$ for prismatic slip. If the grain is refined from 25.5 to 6.8 μm, the increment of yield strength for slip is 44 MPa. However, the area fraction of DRXed grains is only 20% at the edge position (see Fig. 4(b)). According to a simple mixture rule, the increment in overall yield strength will be cut by 80%. For the edge position, the increment in yield strength might be 8.8 MPa. From edge position to center position, the amount of DRXed grain gradually decreases from 20% to 0. Thus, the contribution of refinement hardening might be low to the yield strength.

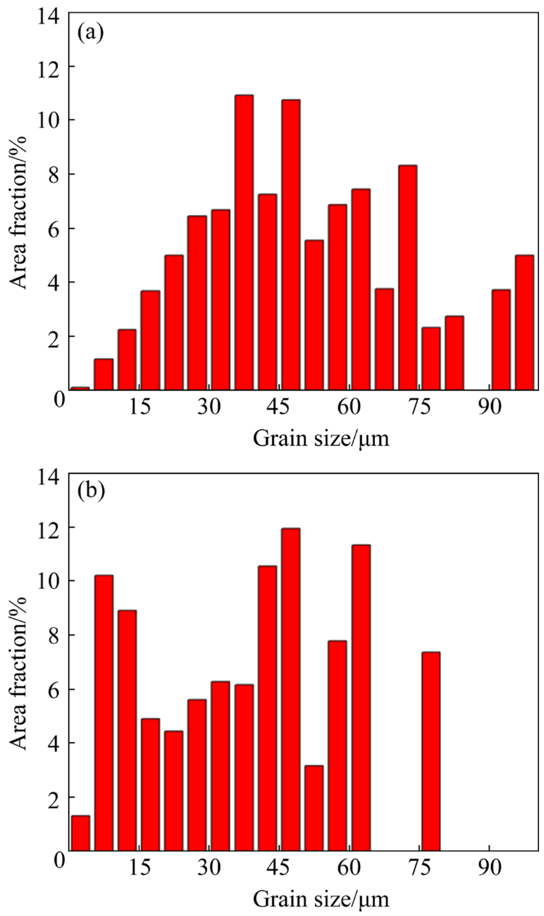

Fig. 4 Grain size distribution of AE sample (a), and edge position of FRT sample (b)

Figure 1 shows that the forward-reverse torsion exhibits little effect on the major texture component. However, this major texture component may be from un-DRXed grains due to the high volume fraction. To further reveal the effect of dynamic recrystallization on the texture, the fine DRXed grains and the coarse un-DRXed grains were extracted separately to draw the pole figures, which are shown in Fig. 5. For the AE sample, the grains with various grain sizes have a similar texture distribution, i.e., strong extrusion texture. For the FRT sample, the coarse grains with size above 15 μm have a similar texture distribution with AE sample. In contrast, the DRXed grains less than 15 μm have a weaker extrusion texture and more disperse texture distribution. The Schmid factor (SF) for basal slip along the ED direction is also shown in Fig. 5. It indicates that the DRXed grains in FRT sample have a higher SF for basal slip than the coarse grains. Generally, the increase in the SF for basal slip will reduce the yield strength owing to its low critical resolved shear stress (CRSS) [43]. However, the grain refinement will increase the CRSS of basal slip for DRXed grains. It has reported that the *k* value of Hall−Petch for basal slip is 158 MPa·$\mu m^{1/2}$ [44]. Thus, when the grain size changes from 25.5 to 6.8 μm, the increment of Hall−Petch in CRSS for basal slip is 29 MPa. It is well known that the activation stress for basal slip can be calculated by the ratio of CRSS to SF. Clearly, only when the CRSS for basal slip of initial grains (25.5 μm) is above 44 MPa, the texture softening of DRXed grains can reduce the activation stress of basal slip. It has been reported that the CRSS of basal slip is usually far lower than that for the AZ31 alloys with a grain size of ~25 μm [45]. Thus, it is considered that the activation stress for basal slip in DRXed grains is still far higher than that in un-DRXed grains. Moreover, the SF of prismatic slip in DRXed grains is slightly less than that in un-DRXed grains. Thus, it is inferred that the change of texture may increase the activation stress by prismatic slip.

Although hot torsion shows little influence on yield strength, it largely increases the tensile ductility and toughness, as shown in Fig. 3. In fact, tensile ductility and toughness are closely related to the strain hardening behavior. It has been reported that the linear decrease in the strain hardening rate is related to dynamic recovery (see Fig. 3(b)) [46]. It has been reported that texture, initial dislocations and grain size will influence the strain hardening behavior [46−48]. Grain refinement and initial dislocations usually enhance the dynamic recovery by promoting annihilation of dislocations [46,49]. However, the FRT sample containing fine grains and initial dislocations exhibits a higher strain hardening rate than the AE sample. Here, the higher strain hardening rate might be attributed to the formation of gradient bimodal grain structure in FRT sample. It has been reported that both gradient microstructure and bimodal microstructure exhibit deformation characteristics of hetero-structures [16,20]. The heterogeneous deformation will generate an additional stress to increase strength and strain hardening capability [15,16].

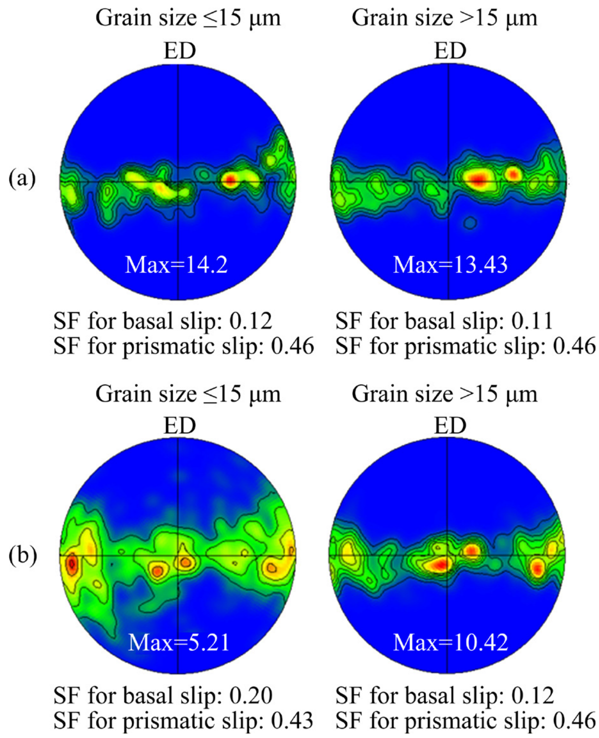

Fig. 5 Pole figures and SF values for various slip systems of hot torsion-deformed samples: (a) AE sample; (b) Edge position of FRT sample

In order to further reveal the deformation characteristics of bimodal microstructure, the EBSD data of the samples stretched to 3% strain are shown in Fig. 6. No twin is detected in the stretched samples. This indicates that slip is the dominant deformation mechanism for two samples. Dislocation slip can cause local rotation of the lattice. For Mg alloys with hexagonal close-packed (HCP) structure, basal $\langle a \rangle$ slip, prismatic $\langle a \rangle$ slip and pyramidal II $\langle c+a \rangle$ slip induce lattice rotation around the $\langle 1\bar{1}00 \rangle$, $\langle 0001 \rangle$ and $\langle 10\bar{1}2 \rangle$ axes, respectively [50]. Thus, the activation of dominant slip system during deformation can be analyzed based on the in-grain misorientation axes (IGMA) analysis. In general, the misorientation angle of 0.5°−2° was used in the IGMA analysis [50]. The results are shown in Fig. 7. For the AE sample, after being stretched 3% strain, the preferred distribution of IGMA around the $\langle 0001 \rangle$ axis is formed. This indicates that prismatic slip was favorably activated. Moreover, the preferred distribution of IGMA around the $\langle 1\bar{1}00 \rangle$ axis can also be observed. This indicates basal slip might be activated at the beginning of plastic deformation owing to its low CRSS.

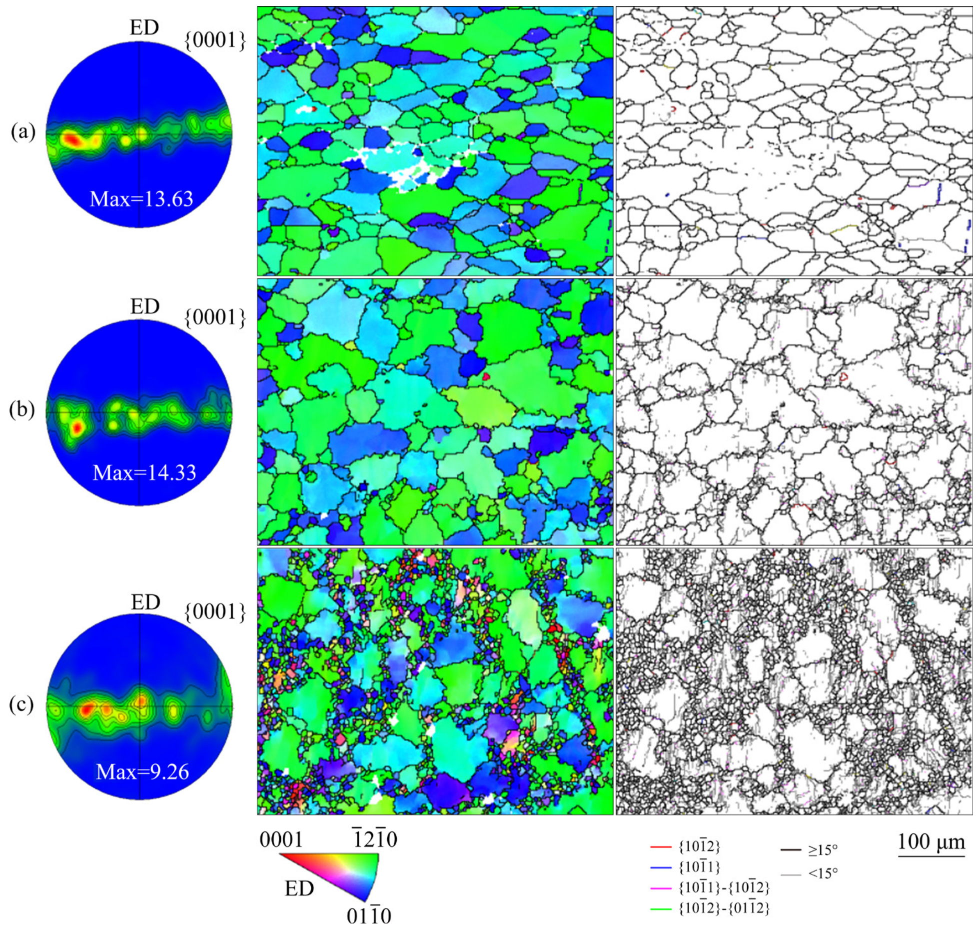

Fig. 6 Pole figures and EBSD maps of samples stretched to 3% strain: (a) AE sample; (b) Center position of FRT sample; (c) Edge position of FRT sample

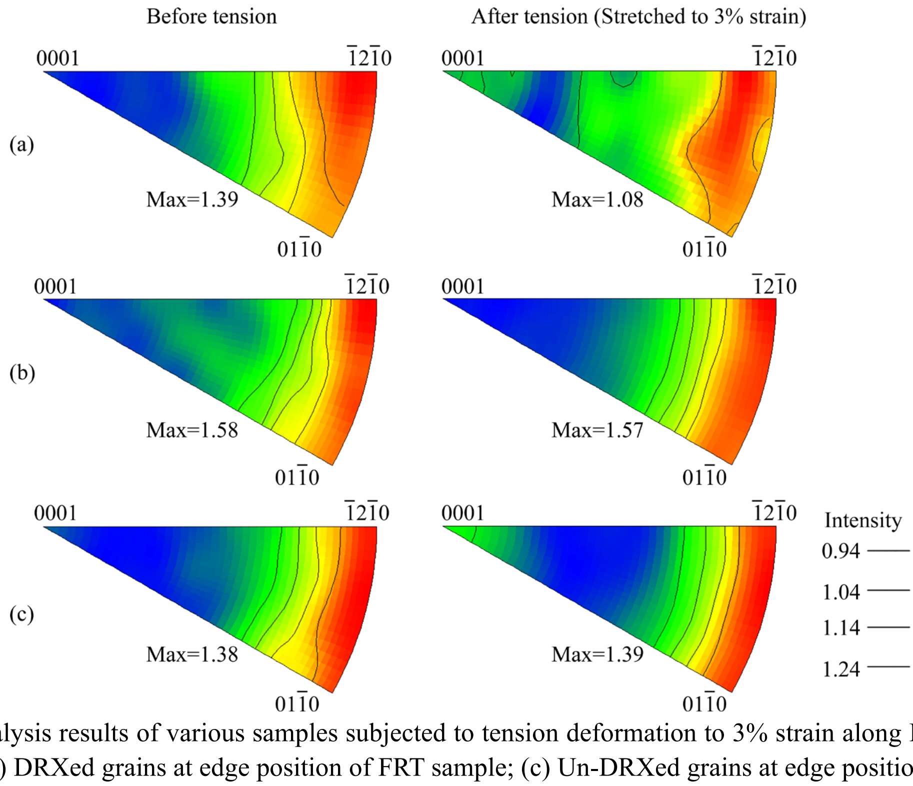

Fig. 7 IGMA analysis results of various samples subjected to tension deformation to 3% strain along ED: (a) All grains in AE sample; (b) DRXed grains at edge position of FRT sample; (c) Un-DRXed grains at edge position of FRT sample

Compared with AE sample, the FRT sample shows a higher intensity in the $\langle 1\bar{1}00\rangle$ axis in the IGMA analysis. It further confirms that basal slip is profusely activated during hot torsion. After being stretched to 3% strain, un-DRXed grains and DRXed grains exhibit different IGMA distribution in the FRT sample. For the coarse un-DRXed grains, the intensity of $\langle 0001\rangle$ axis in the IGMA analysis is enhanced by stretched to 3% strain. This indicates that prismatic slip dominates the early deformation. However, there is not any concentration on the $\langle 0001\rangle$ axis for the IGMA analysis of the fine DRXed grains. This indicates that the prismatic slip in fine DRXed grains is harder to activate than that in coarse grains. Thus, present bimodal structure exhibits the characteristics of heterogeneous structure, and the bimodal structure has a gradient distribution along the radius direction. It has been reported that bimodal structure and gradient structure can generate HDI stress to increase the stain hardening rate [15,16].

HDI stress can be analyzed by the loading−unloading−reloading (LUR) tests [16], as shown in Fig. 8(a). Figure 8(b) shows the enlarged hysteresis loops from Fig. 8(a). It notes that both AE and FRT samples show hysteresis loops during LUR tests. In contrast, the FRT sample with gradient bimodal structure shows a more pronounced loop. It has been reported that the HDI stress is the driving force for the reversal of mobile dislocations during the unloading. Meanwhile, HDI stress acts as resistance to dislocation sliding forward during the reloading. Thus, higher HDI stress corresponds to lager Bauschinger effect [15,16]. Clearly, FRT sample exhibits larger Bauschinger effect and a higher HDI stress than AE sample. It is worth noting that AE sample with homogeneous micro-structure also produces heterogeneous deformation. As shown in Fig. 4(a), the grain size in the AE samples is also not absolutely uniform. Moreover, the plasticity anisotropy caused by textures and the pinning effect via solute atoms, precipitates and

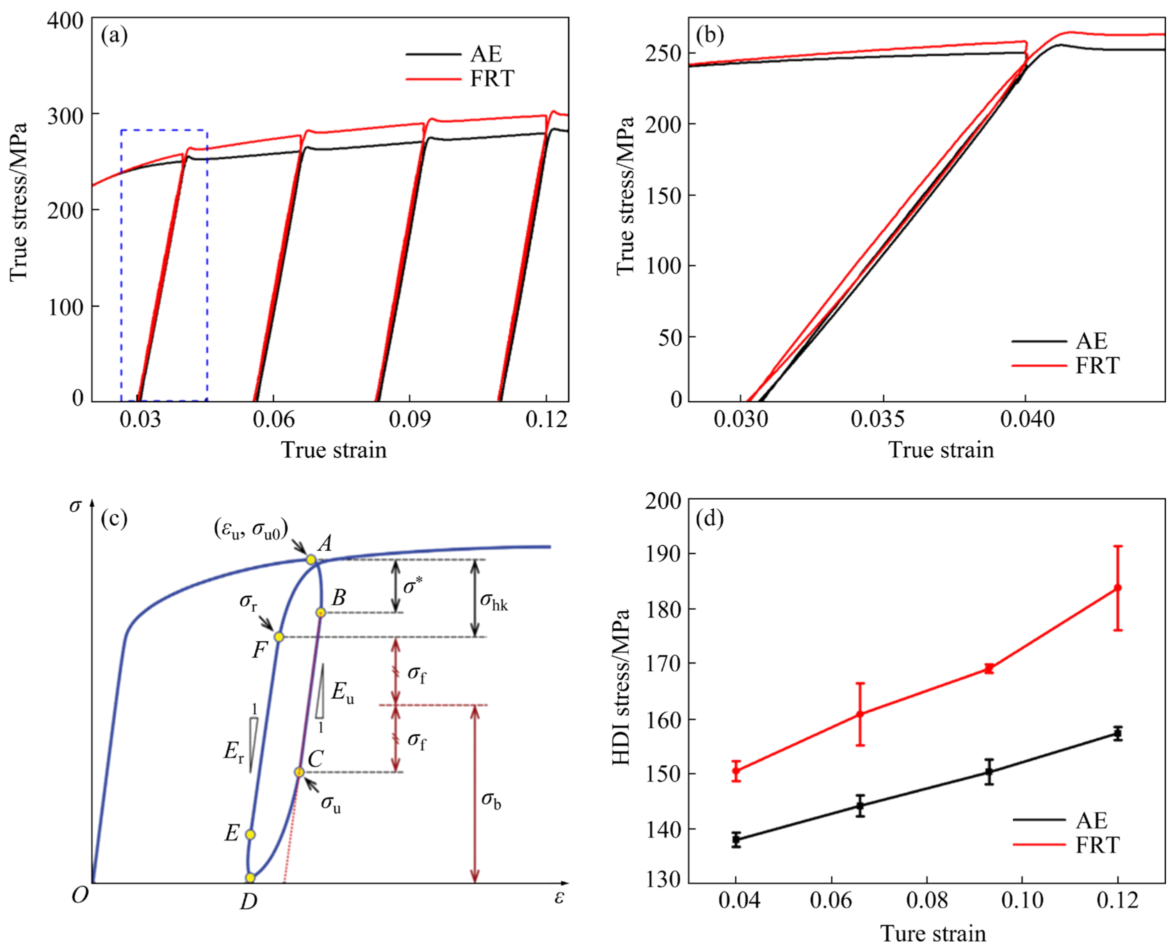

Fig. 8 (a) Unloading and reloading test hysteresis loops measured at various tensile strains; (b) Enlarged hysteresis loops from (a); (c) Schematic diagram for calculating HDI stress [16]; (d) Calculated HDI stress based on hysteresis loops of both samples

grain boundaries can cause non-uniform deformation characteristics [51−53]. Obviously, prominent heterogeneity of microstructure in FRT sample exacerbates the heterogeneous deformation.

According to a previous study, HDI stress can be evaluated based on hysteresis loops, as shown in Fig. 8(c) [16]. Herein, the effective unloading Young's modulus (E_u) and the effective reloading Young's modulus (E_r) are assumed to be equal quantities during the LUR test. HDI stress (σ_{HDI}) can be calculated by the following formula:

$$\sigma_{HDI}=(\sigma_u+\sigma_r)/2 \tag{2}$$

where a 5% slope reduction from the effective Young's modulus is used to determine the σ_u (the unloading yield point) and σ_r (the reloading yield point). The change of HDI stress as a function of true strain is shown in Fig. 8(d). For both samples, the HDI stress increases with the increase of strain. However, HDI stress of the FRT samples is higher than that of the AE samples over the entire tensile strain range. Based on above discussion, it has been found that fine DRXed grains are harder than the coarse un-DRXed grains. This will lead to the deformation inhomogeneity during continuous deformation. The strain gradient caused by the inhomogeneity of the deformation needs to be coordinated by the geometrically necessary dislocations, which will produce obvious HDI stress [15,17]. In this work, the high HDI stress will be responsible for the enhanced strain hardening rate and tensile ductility [16].

The current study has demonstrated that the preparation of bimodal Mg alloys by hot torsion is beneficial to improving the tensile properties. In addition, the HDI hardening effect via the gradient bimodal structure greatly depends on the relative volume fraction of coarse and fine grains and their distribution [15−17]. In the following study, the gradient bimodal structure will be further optimized by adjusting the torsion parameters to achieve further improvement in strength and ductility. Moreover, textured Mg alloys generally exhibit plastic anisotropy [9]. The effect of torsion deformation on compressive anisotropy of extruded AZ31 rod has been investigated [54]. Although the reciprocating torsion did not change the texture of the as-extruded AZ31 rods, the formation of the bimodal structure may also affect the anisotropy. Therefore, in the follow-up work, the effect of such a gradient bimodal structure on the anisotropy will also become a research topic.

4 Conclusions

(1) FRT process has little influence on texture, while induces incomplete dynamic recrystallization. This results in the formation of bimodal microstructure in which coarse grains are surrounded by fine recrystallized grains. Due to the characteristic of torsion deformation, the bimodal structure with gradient distribution along the radial direction is formed in FRT sample.

(2) Compared to coarse un-DRXed grains, fine DRXed grains have a weaker extrusion texture and higher SF for basal slip. However, fine DRXed grains still remain higher yield stress owing to the strong Hall−Petch hardening effect.

(3) The bimodal structure has little influence on the yield strength due to the low volume fraction of fine DRXed grains, however largely increases the peak stress and tension ductility. It is mainly attributed to the formation of high HDI stress from the deformation inhomogeneity between fine DRXed grains and coarse un-DRXed grains.

Acknowledgments

This work was financially supported by the Natural Science Foundation of Chongqing, China (No. cstc2021jcyj-msxmX0433), the Chongqing Foundation of Science and Technology, China (Nos. cstc2020jxjlX0001, cstc2021jxjl50004), and the National Natural Science Foundation of China (No. 51601154). The authors acknowledge Mr. Zhi-wen DU for the EBSD and tensile experiments.

References

[1] JAVAID A, CZERWINSKI F. Progress in twin roll casting of magnesium alloys: A review [J]. Journal of Magnesium and Alloys, 2021, 9: 362−391.

[2] CAO Li-jie, MA Guo-rui, WANG Chun-xia, CHEN Zheng-jian, ZHANG Jia-heng. Effect of compression ratio on microstructure evolution of Mg−10%Al−1%Zn−1%Si alloy prepared by SIMA process [J]. Transactions of Nonferrous Metals Society of China, 2021, 31: 2597−2605.

[3] CHANG Li-li, GUO Jing, SU Xiao-jing. Effect of Y on microstructure evolution and mechanical properties of Mg−4Li−3Al alloys [J]. Transactions of Nonferrous Metals Society of China, 2021, 31: 3691−3702.

[4] LI Xiao-qiang, REN Liang, LE Qi-chi, BAO Lei, JIN

Pei-peng, WANG Ping, CHENG Chun-long, ZHOU Xiong, HU Cheng-lu. Reducing the yield asymmetry in Mg−5Li−3Al−2Zn alloy by hot-extrusion and multi-pass rolling [J]. Journal of Magnesium and Alloys, 2021, 9: 937−949.

[5] SONG Bo, DU Zhi-wen, YANG Qing-shan, GUO Ning, GUO Sheng-feng, YU Jin-cheng, XIN Ren-long. Effect of pre-rolling path on mechanical properties of rolled ZK60 alloys [J]. Transactions of Nonferrous Metals Society of China, 2021, 31(5): 1322−1338.

[6] LU Li-wei, LIU Tian-mo, CHEN Yong, WANG Zhong-chang. Deformation and fracture behavior of hot extruded Mg alloys AZ31 [J]. Materials Characterization, 2012, 67: 93−100.

[7] YAN Zhao-ming, LI Xu-bin, ZHENG Jie, ZHANG Zhi-min, WANG Qiang, XU Kai-hua, FAN Hong-zhi, ZHANG Guan-shi, ZHU Jia-xuan, XUE Yong. Microstructure evolution, texture and mechanical properties of a Mg−Gd−Y−Zn−Zr alloy fabricated by cyclic expansion extrusion with an asymmetrical extrusion cavity: The influence of passes and processing route [J]. Journal of Magnesium and Alloys, 2021, 9: 964−982.

[8] SHI Zhi-ming, KIM W J, CAO Fu-yong, DARGUSCH M S, ATRENS A. Stress corrosion cracking of high-strength AZ31 processed by high-ratio differential speed rolling [J]. Journal of Magnesium and Alloys, 2015, 3: 271−282.

[9] KIM W J, YOO S J, CHEN Z H, JEONG H T. Grain size and texture control of Mg−3Al−1Zn alloy sheet using a combination of equal-channel angular rolling and high-speed-ratio differential speed-rolling processes [J]. Scripta Materialia, 2009, 60: 897−900.

[10] FAN Ling-ling, ZHOU Ming-yang, GUO Yang-yang, ZHANG Yu-wen-xi, QUAN Gao-feng. Effect of ECAP process on liquid distribution of AZ80M alloy during semi-solid isothermal heat treatment [J]. Transactions of Nonferrous Metals Society of China, 2021, 31: 1599−1611.

[11] WANG Bo-ning, WANG Feng, WANG Zhi, LIU Zheng, MAO Ping-li. Fabrication of fine-grained, high strength and toughness Mg alloy by extrusion-shearing process [J]. Transactions of Nonferrous Metals Society of China, 2021, 31: 666−678.

[12] LIU Shuai-shuai, WANG Wei-zhang, CHEN Xiang, HUANG Guang-sheng, LIU Han, TANG Ai-tao, JIANG Bin, PAN Fu-sheng. Enhanced strength and ductility of AZ91 alloy with heterogeneous lamella structure prepared by pre-aging and low-temperature extrusion [J]. Materials Science and Engineering A, 2021, 812: 141094.

[13] HAN Ting-zhuang, ZOU Jing-feng, HUANG Guang-sheng, MA Li-feng, CHE Chao-jie, JIA Wei-tao, WANG Li-fei, PAN Fu-sheng. Improved strength and ductility of AZ31B Mg alloy sheets processed by accumulated extrusion bonding with artificial cooling [J]. Journal of Magnesium and Alloys, 2021, 9: 1715−1724.

[14] LIU Shuai-shuai, ZHANG Jun-lei, CHEN Xiang, HUANG Guang-sheng, XIA Da-biao, TANG Ai-tao, ZHU Yun-tian, JIANG Bin, PAN Fu-sheng. Improving mechanical properties of heterogeneous Mg−Gd alloy laminate via accumulated extrusion bonding [J]. Materials Science and Engineering A, 2020, 785: 139324.

[15] WU Xiao-lei, ZHU Yun-tian. Heterogeneous materials: A new class of materials with unprecedented mechanical properties [J]. Materials Research Letters, 2017, 5: 527−532.

[16] YANG Mu-xin, PAN Yue, YUAN Fu-ping, ZHU Yun-tian, WU Xiao-lei. Back stress strengthening and strain hardening in gradient structure [J]. Materials Research Letters, 2016, 4: 145−151.

[17] ZHU Yun-tian, WU Xiao-lei. Perspective on hetero-deformation induced (HDI) hardening and back stress [J]. Materials Research Letters, 2019, 7: 393−398.

[18] CHEN Xiang, WANG Wei-zhang, ZHANG Jun-lei, HUANG Guang-sheng, LIU Shuai-shuai, TANG Ai-tao, JIANG Bin, PAN Fu-sheng. Tailoring AZ91 laminates for combination of strength and ductility [J]. Transactions of Nonferrous Metals Society of China, 2021, 31: 3703−3718.

[19] WANG Qing-hang, SHEN Ya-qun, JIANG Bin, TANG Ai-tao, SONG Jiang-feng, JIANG Zhong-tao, YANG Tian-hao, HUANG Guang-sheng, PAN Fu-sheng. Enhanced stretch formability at room temperature for Mg−Al−Zn/Mg−Y laminated composite via porthole die extrusion [J]. Materials Science and Engineering A, 2018, 731: 184−194.

[20] ZHANG Hang, WANG Hui-yuan, WANG Jin-guo, RONG Jian, ZHA Min, WANG Cheng, MA Pin-kui, JIANG Qi-chuan. The synergy effect of fine and coarse grains on enhanced ductility of bimodal-structured Mg alloys [J]. Journal of Alloys and Compounds, 2019, 780: 312−317.

[21] WANG Bao-jie, XU Dao-kui, SHENG Li-yuan, HAN En-hou, SUN Jie. Deformation and fracture mechanisms of an annealing-tailored “bimodal” grain-structured Mg alloy [J]. Journal of Materials Science & Technology, 2019, 35: 2423−2429.

[22] SONG Bo, PAN Hu-cheng, CHAI Lin-jiang, GUO Ning, ZHAO Huai-zhi, XIN Ren-long. Evolution of gradient microstructure in an extruded AZ31 rod during torsion and annealing and its effects on mechanical properties [J]. Materials Science and Engineering A, 2017, 689: 78−88.

[23] SONG Bo, WANG Meng, SHI Ruo-lan, DU Zhi-wen, GUO Ning, WANG Fang, GUO Sheng-feng. Promoting hybrid twins structure to reduce yield asymmetry of rolled AZ31 plates by combining side-rolling and torsion [J]. Journal of Magnesium and Alloys, 2023, 6: 2096−2105.

[24] GUO Ning, SONG Bo, YU Hong-bing, XIN Ren-long, WANG Bing-shu, LIU Ting-ting. Enhancing tensile strength of Cu by introducing gradient microstructures via a simple torsion deformation [J]. Materials & Design, 2016, 90: 545−550.

[25] GU Ji, ZHANG Li-xin, TANG Ya-hui, SONG Min, NI Song, AN Xiang-hai, DU Yong, LI Zhou, LIAO Xiao-zhou. Improving the strength and retaining the ductility of microstructural graded coarse-grained materials with low stacking fault energy [J]. Materials & Design, 2018, 160: 21−33.

[26] GUO Ning, ZHAO Ying-long, LONG Shi-teng, SONG Bo, HU Jian-jun, GAN Bin, CHAI Lin-jiang, GUO Sheng-feng. Microstructure and mechanical properties of $(CrCoNi)_{97}$-$Al_{1.5}Ti_{1.5}$ medium entropy alloy twisted by free-end-torsion at room and cryogenic temperatures [J]. Materials Science and Engineering A, 2020, 797: 140101.

[27] PAN Qing-song, ZHANG Liang-xue, FENG Rui, LU Qiu-hong, AN Ke, CHUANG A C, POPLAWSKY J D, LIAW P K, LU Lei. Gradient cell-structured high-entropy alloy with exceptional strength and ductility [J]. Science, 2021, 374: 984−989.

[28] WEI Yu-jie, LI Yong-qiang, ZHU Lian-chun, LIU Yao, LEI Xian-qi, WANG Gang, WU Yan-xin, MI Zhen-li, LIU Jia-bin, WANG Hong-tao, GAO Hua-jian. Evading the strength–ductility trade-off dilemma in steel through gradient hierarchical nanotwins [J]. Nature Communications, 2014, 5: 3580.

[29] GUO Ning, ZHANG Zhi-min, DONG Qing-shan, YU Hong-bing, SONG Bo, CHAI Lin-jiang, LIU Cong, YAO Zhong-wen, DAYMOND M R. Strengthening and toughening austenitic steel by introducing gradient martensite via cyclic forward/reverse torsion [J]. Materials & Design, 2018, 143: 150−159.

[30] BISWAS S, BEAUSIR B, TOTH L S, SUWAS S. Evolution of texture and microstructure during hot torsion of a magnesium alloy [J]. Acta Materialia, 2013, 61: 5263−5277.

[31] CHEN Hong-bing, SONG Bo, GUO Ning, LIU Ting-ting, ZHOU Tao, HE Jie-jun. Dynamic recrystallization and grain refinement in extruded AZ31 rod during hot torsion deformation at 150 °C [J]. Metals and Materials International, 2019, 25: 147−158.

[32] GUO X Q, WU W, WU P D, QIAO H, AN K, LIAW P K. On the Swift effect and twinning in a rolled magnesium alloy under free-end torsion [J]. Scripta Materialia, 2013, 69: 319−322.

[33] BEAUSIR B, TÓTH L S, NEALE K W. Ideal orientations and persistence characteristics of hexagonal close packed crystals in simple shear [J]. Acta Materialia, 2007, 55: 2695−2705.

[34] SONG BO, SHU Xiao-gang, PAN Fu-sheng, LI Guo-qiang, GUO Ning, LIU Ting-ting, CHAI Lin-jiang, XIN Ren-long. Influence of torsion route on the microstructure and mechanical properties of extruded AZ31 rods [J]. Advanced Engineering Materials, 2017, 19: 1700267.

[35] XU S W, KAMADO S, MATSUMOTO N, HONMA T, KOJIMA Y. Recrystallization mechanism of as-cast AZ91 magnesium alloy during hot compressive deformation [J]. Materials Science and Engineering A, 2009, 527: 52−60.

[36] PARK C H, OH C S, KIM S. Dynamic recrystallization of the H- and O-tempered Mg AZ31 sheets at elevated temperatures [J]. Materials Science and Engineering A, 2012, 542: 127−139.

[37] LI Na-li, HUANG Guang-jie, ZHONG Xiao-yu, LIU Qing. Deformation mechanisms and dynamic recrystallization of AZ31 Mg alloy with different initial textures during hot tension [J]. Materials & Design, 2013, 50: 382−391.

[38] ZHANG Hua, BAI Xiao-qing, HOU Min-jian, WANG Li-fei, ZHANG Qiang, FAN Jian-feng, WU Yu-cheng, DONG Hong-biao, XU Bing-she. Enhancing compressive mechanical properties of rolled AZ31 Mg alloy plates by pre-compression [J]. Materials Science and Engineering A, 2020, 772: 138686.

[39] DEL VALLE J A, RUANO O A. Influence of texture on dynamic recrystallization and deformation mechanisms in rolled or ECAPed AZ31 magnesium alloy [J]. Materials Science and Engineering A, 2008, 487: 473−480.

[40] SONG Bo, XIN Ren-long, SUN Li-yun, CHEN Gang, LIU Qing. Enhancing the strength of rolled ZK60 alloys via the combined use of twinning deformation and aging treatment [J]. Materials Science and Engineering A, 2013, 582: 68−75.

[41] YU Hui-hui, XIN Yun-chang, WANG Mao-yin, LIU Qing. Hall−Petch relationship in Mg alloys: A review [J]. Journal of Materials Science & Technology, 2018, 34: 248−256.

[42] YU Hui-hui, LI Chang-zheng, XIN Yun-chang, CHAPUIS A, HUANG Xiao-xu, LIU Qing. The mechanism for the high dependence of the Hall−Petch slope for twinning/slip on texture in Mg alloys [J]. Acta Materialia, 2017, 128: 313−326.

[43] SONG Bo, XIN Ren-long, GUO Ning, CHEN Zhi-qian, YANG Xiao-fang, LIU Qing. Influence of basal slip activity in twin lamellae on mechanical behavior of Mg alloys [J]. Materials Letters, 2016, 176: 147−150.

[44] WANG Y, CHOO H. Influence of texture on Hall−Petch relationships in an Mg alloy [J]. Acta Materialia, 2014, 81: 83−97.

[45] TAM K J, VAUGHAN M W, SHEN L M, KNEZEVIC M, KARAMAN I, PROUST G. Modelling the temperature and texture effects on the deformation mechanisms of magnesium alloy AZ31 [J]. International Journal of Mechanical Sciences, 2020, 182: 105727.

[46] DEL VALLE J A, CARREÑO F, RUANO O A. Influence of texture and grain size on work hardening and ductility in magnesium-based alloys processed by ECAP and rolling [J]. Acta Materialia, 2006, 54: 4247−4259.

[47] GUO Li-li, CHEN Zhong-chun, GAO Li. Effects of grain size, texture and twinning on mechanical properties and work-hardening behavior of AZ31 magnesium alloys [J]. Materials Science and Engineering A, 2011, 528: 8537−8545.

[48] SONG Bo, XIN Ren-long, CHEN Gang, ZHANG Xi-yan, LIU Qing. Improving tensile and compressive properties of magnesium alloy plates by pre-cold rolling [J]. Scripta Materialia, 2012, 66: 1061−1064.

[49] AFRIN N, CHEN D L, CAO X, JAHAZI M. Strain hardening behavior of a friction stir welded magnesium alloy [J]. Scripta Materialia, 2007, 57: 1004−1007.

[50] CHUN Y B, DAVIES C H J. Investigation of prism ⟨*a*⟩ slip in warm-rolled AZ31 alloy [J]. Metallurgical and Materials Transactions A, 2011, 42: 4113−4125.

[51] KASSNER M E, GEANTIL P, LEVINE L E. Long range internal stresses in single-phase crystalline materials [J]. International Journal of Plasticity, 2013, 45: 44−60.

[52] WANG Yan-fei, YANG Mu-xin, MA Xiao-long, WANG Ming-sai, YIN Kun, HUANG Ai-hui, HUANG Chong-xiang. Improved back stress and synergetic strain hardening in coarse-grain/nanostructure laminates [J]. Materials Science and Engineering A, 2018, 727: 113−118.

[53] LIU Shuai-shuai, CHEN Yi-fan, YANG Hong, HUANG Guang-sheng, CHEN Xian-hua, TANG Ai-tao, JIANG Bin, PAN Fu-sheng. Revealing the role of heterostructural parameters in hetero-deformation induced stress of Mg−13Gd alloy [J]. Materials Science and Engineering A, 2022, 839: 142844.

[54] DU Zhi-wen, SONG Bo, GUO Ning, LIU Ting-ting, GUO sheng-feng, XIN Ren-long. Revealing the texture evolution and compressive anisotropy in free-end twisted AZ31 rods [J]. Journal of Materials Engineering and Performance, 2021, 30: 1157−1166.

引入梯度双模态组织提升挤压态 AZ31 棒材的拉伸性能

尚 琦[1]，吴 凡[1]，陈红兵[2]，张红菊[3]，刘婷婷[1]，郭 宁[1]，郭胜锋[1]，宋 波[1]

1. 西南大学 材料与能源学院，重庆 400715；
2. 西南大学 工程技术学院，重庆 400715；
3. 西南大学 分析测试中心，重庆 400715

摘 要：利用 350 ℃下的往复扭转制备具有梯度双模态显微组织的镁合金棒。详细研究双模态显微组织对合金拉伸性能和变形机制的影响。梯度双模态显微组织的形成归因于不完全动态再结晶和扭转变形的特点。双模态结构对屈服强度的影响较小，但极大增加了峰值应力和拉伸延展性。由梯度双模态显微组织产生的大异质变形诱导的强化是应变硬化能力和拉伸延展性提升的原因。最后，讨论了相关的变形机制。

关键词：镁合金；热扭转；双模态显微组织；异质变形；拉伸性能

(Edited by Wei-ping CHEN)